Influence of Macro-Topography on Mechanical Performance of 1.0 wt% Nanoclay/Multi-Layer Graphene-Epoxy Nanocomposites

Rasheed Atif and Fawad Inam*

Northumbria University, Faculty of Engineering and Environment, Department of Mechanical and Construction Engineering, Newcastle upon Tyne NE1 8ST, United Kingdom.

E-mail: fawad.inam@northumbria.ac.uk (Tel.: +44 1912273741)

Abstract: Influence of topography on the variation in mechanical performance of 1.0 wt% Multi-Layer Graphene (MLG)/nanoclay-epoxy samples has been investigated. Three different systems were produced: 1.0 wt% MLG-EP, 1.0 wt% nanoclay-EP, and 0.5 wt% MLG-0.5 wt% nanoclay-EP. The influence of synergistic effect on mechanical performance in case of hybrid nanocomposites is also studied. Various topography parameters studied include maximum roughness height (R_z or R_{max}), root mean square value (R_q), roughness average (R_a), and surface waviness (W_a). The R_z of as-cast 1.0 wt% MLG, nanoclay, and 0.5 wt% MLG-0.5 wt% nanoclay-EP nanocomposites were 41.43 µm, 43.54 µm, and 40.28 µm, respectively. The 1200P abrasive paper and the velvet cloth decreased the R_z value of samples compared with as-cast samples. In contrary, the 60P and 320P abrasive papers increased the R_z values. Due to the removal of material from the samples by erosion, the dimensions of samples decreased. The weight loss due to erosion was commensurate with the coarseness of abrasive papers. It was recorded that MLG is more influential in enhancing the mechanical performance of epoxy nanocomposites than nanoclay. Additionally, it was observed that mechanical performance of hybrid nanocomposites did not show a marked difference suggesting that synergistic effects are not strong enough in MLG and nanoclay.

Keywords: Topography; mechanical performance; fracture toughness; 1.0 wt% MLG/nanoclay-epoxy nanocomposites; dynamic mechanical performance.

1. Introduction:

The tribological prevention of thermosetting polymers is getting proliferating attention to use these polymers in mechanical engineering and construction related fields [1–5]. To comprehend esoteric phenomena of fracture mechanics and tribology, it is of utmost significance to investigate the correlation between bulk properties and the topographical features of the thermosetting polymers [6]. To enhance resistance against wear, surface coatings are applied on the monolithic polymers. It is due to the preferential growth of crystals that close the fissures and offers the choice to fix the topographical features apposite to the service conditions [7–10]. Various coating methods include electrochemical/galvanic deposition and thermal and plasma spraying that can produce heavy coatings of high load support [11].

Although marked adhesive strength between substrate and the coating might be attained in as-coated samples, nevertheless, delamination is a possible occurrence when the samples undergo any external forces. It is due to the fact that the coatings have very high stiffness values and very low plastic deformability to track the change in the shape and dimensions of the substrate. This limitation may be aggravated in case of elevated temperatures and/or thermal stresses because of the large difference in the coefficients of thermal expansion (CTE) of substrate and the coating. For instance, epoxy may present ten times more expansion when subjected to thermal cycling than most of the thin film materials investigated [11]. On the other hand, coatings of polymers on the polymer substrate may have similar CTE and stiffness values; nevertheless, these coatings crash in applications where wear and erosion might take place. Hence, even if coated, there is high probability that the polymers will undergo wear in cases where sliding contact

is inescapable. Therefore, it gets important to enhance the performance of the monolithic polymers, such as epoxy, for tribological applications. The tribological properties of epoxy can be enhanced with the addition of (nano-) fillers like metallic oxides [12–14], clays [15–17], carbon nanotubes (CNTs) [18–20], and other carbonaceous materials [21–23].

The mechanical performance of polymers can be significantly improved with the incorporation of nano-fillers [24–27]. When multiple nano-fillers are dispersed in the polymer matrix, synergistic effects come into play [28]. Due to synergistic effects, the dispersion state of hybrid nano-fillers becomes better than when single nano-filler is used. It helps improve the physical and mechanical performances of hybrid nanocomposites. Sumfleth et al. produced MWNT-epoxy nanocomposites and doped the system with titania [28]. They reported that the dispersion state of nano-fillers improved in multiphase nanocomposites. Similarly, Ma et al. produced CNT-acrylonitrile butadiene styrene (ABS) nanocomposites and doped them with nanoclay [29]. They also observed a better dispersion state of the nano-fillers. It was further reported that nanoclay is also effective in improving the dispersion state of CNT in CNT-polyamide nanocomposites. It was concluded that titania can enhance the dispersion state more than that by block copolymers. A large volume fraction of CNT can be uniformly dispersed by using titania. The extent of improvement in the dispersion state of a nano-filler by another nano-filler is dependent on the extent of synergistic effects caused by hybrid nano-fillers.

The mechanical interlocking can improve the interfacial interactions in the nanocomposites [30]. In addition, the capillary wetting of the fillers by the polymers can be enhanced by making the fillers more hairy, rough, and hierarchical [31]. Due to the polymer wetting and mechanical interlocking of fillers with rough surfaces, the fiber-matrix interphase is strengthened by local reinforcement [32]. As the topography is influential at the interphase level, similarly, the topography of bulk nanocomposites is of equal importance. At one side, it is important in tribological applications as the co-efficient of friction is significantly dependent upon the surface condition [33–36]. On the other side, the mechanical performance of sole nanocomposites is also dependent on topography. When the surfaces contain notches, the notches generate triaxial state of stress under which the mechanical performance severely degrades [37]. Therefore, detailed observation of the influence of topography on mechanical performance of (hybrid) nanocomposites is essential. To the authors' best knowledge, no article is yet published relating the topography, synergistic effects, dispersion state of fillers and mechanical performance of nanocomposites.

In this work, 1.0 wt% MLG/nanoclay-EP samples were processed with abrasive papers to modify the topography. Three compositions were produced: 1.0 wt% MLG-EP, 1.0 wt% nanoclay-EP, and 0.5 wt% MLG-0.5 wt% nanoclay-EP. The influence of synergistic effect on mechanical performance in case of hybrid nanocomposites is also studied. The topography was measured using an Alicona optical microscope. The dynamic mechanical performance, mechanical performance and their variation with topography of samples were investigated. The results indicated that the topography has a significant impact on the aforementioned properties of 1.0 wt% MLG/nanoclay-EP samples. In addition, it was observed that mechanical performance of hybrid nanocomposites did not show a marked difference suggesting that synergistic effects are not strong enough in MLG and nanoclay.

2. Experimental work:

2.1. Materials

MLG (99.2% purity, 80 m^2/g specific surface area, 4.5 µm average lateral size, 12 nm average thickness) used was purchased from Graphene Supermarket, USA. Halloysite nanoclay (30-70 nm diameter, 1-4 µm length, 2.53 g/cm^3 density, 64 m^2/g surface area) was used as second filler and purchased from Sigma-Aldrich. The epoxy and hardeners used were based on bisphenol A-epichlorohydrin and dimethylbenzylamine isophorone diamine, respectively. The resin was purchased from Polyfibre, UK. The densitities of liquid epoxy and hardener were ~1.3 g/cm^3 and ~1.1 g/cm^3, respectively.

2.2. Production of samples

The fillers were shaken in the resin for 3 h using tip sonicator (Model VC 750, Vibra-cell, USA, 750 W, 250 kHz). The epoxy and hardener were degassed in separate beakers for 1 h. The mixing ratio of hardener: epoxy was 1:2 by weight. Following thorough 10 min hand mixing, resin was again degassed for 15 min. Silicone molds were used to cast the samples. Samples were initially cured at room temperature (6 h), and to ensure proper crosslinking, post-curing was carried out at 150 °C (overnight). The abrasive papers were used to treat bottom and top surfaces of samples on grinding wheels at 150 rpm.

2.3. Characterization

ASTM Standard D792 was used to measure densification. The densities of water, hardener, and epoxy were 0.9975, 1.1, and 1.3 g/cm^3, respectively. Vickers microhardness was measured using Buehler Micromet II hardness tester (200 g, 10 s). Universal Testing Machine (Instron Model 3382) was used to conduct tensile test (ASTM D638, 4 mm thickness, Type-V geometry, 0.5 mm/min), three-point bending test (ASTM D790, 3 × 12.7 × 48 mm, 1.0 mm/min), and mode-I fracture toughness test (ASTM D5045, 36 × 6 × 3 mm, crack length 3 mm, 0.5 mm/min). ASTM standard D 6110 was used to measure Charpy impact toughness (specimen dimensions 64 × 12.7 × 3.2 mm with V-notch of 45°, 2.5 mm depth and 0.25 mm tip radius). An Infinite focus Alicona G4 optical microscope was employed to measure topography. The working principle of the microscope is focus-follow method which is a non-contact method. DMA (PerkinElmer, Model 8000, specimen dimensions 30 × 8 × 2.5 mm, temperature range of 60 °C - 180 °C, rate of 5 °C/min, 1 Hz frequency with 10 N force) was used to measure dynamic mechanical performance. The values reported are an average of five specimens and error bars indicate standard deviation.

3. Results and discussion:

The topography of 1.0 wt% MLG-EP samples is highlighted in Figure 1. The roughness values were lowered by processing with 1200P abrasive paper and velvet cloth while enhanced with 320P and 60P. Figure 1 (ai) is the optical micrograph of 1.0 wt% MLG-EP (as-cast). The surface waviness (Figure 1aii) of the nanocomposites fluctuates between ±15 µm while the roughness (Figure 1aiii) fluctuates between ±40 µm. The roughness in as-cast samples is caused by the mold surface. From the roughness chart,

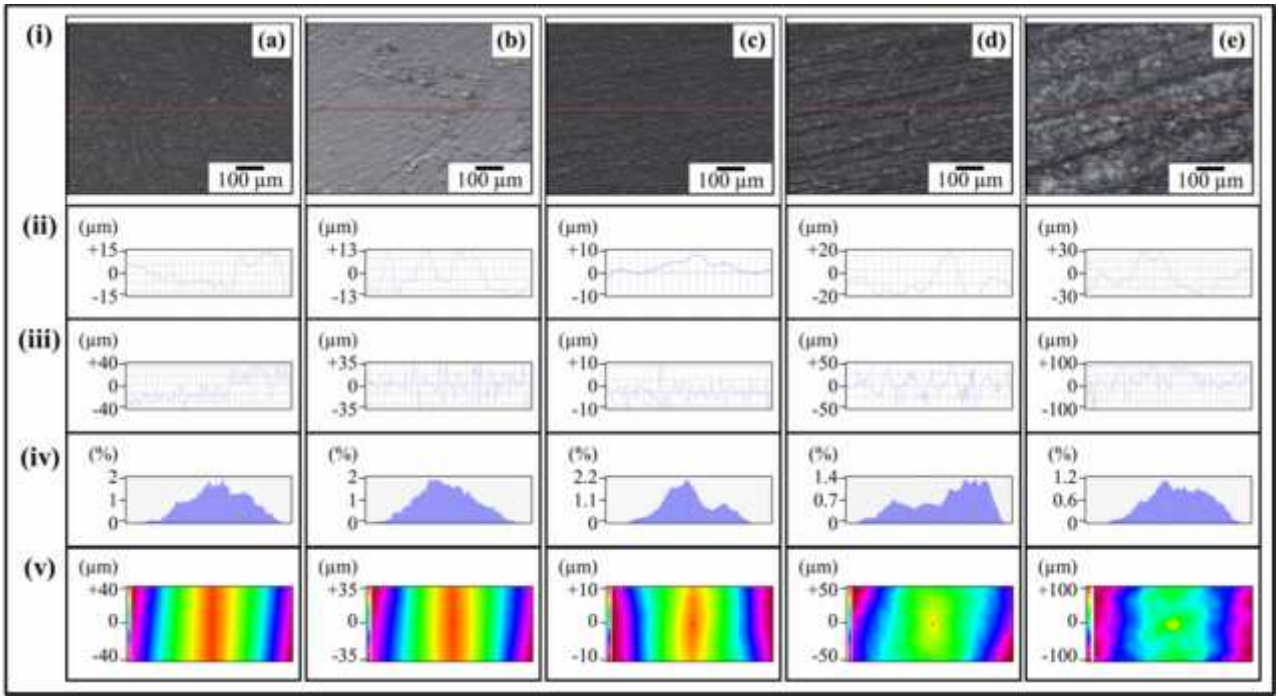

Figure 1. Topography profiles of 1.0 wt% MLG-EP samples: (a) As-cast; (b) Velvet cloth; (c) 1200P; (d) 320P; and (E) 60P abrasive papers. In all cases, (i) optical image, (ii) surface waviness, (iii) surface roughness (selected line), (iv) topographical dimensions vs. percentage, and (v) surface profile of selected region of nanocomposites.

pointed notches of depth of around 40 µm can be observed on the as-cast 1.0 wt% MLG-EP nanocomposites. The Gaussian distribution (Figure 1aiv) indicates a wide distribution of surface roughness with major size fraction of 2%. The roughness profile (Figure 1av) indicates that the roughness mainly lies in the range of ±40 µm with a large notch.

Figure 1 (bi) is the micrograph of 1.0 wt% MLG-EP. The waviness (Figure 1bii) fluctuates between ±13 µm while the roughness (Figure 1biii) fluctuates between ±35 µm. The Gaussian distribution (Figure 1biv) indicates a nearly uniform distribution of roughness size with major size fraction of 2%. A big variation in the roughness can be caused by the diamond paste which was used on the velvet cloth. The roughness profile (Figure 1bv) indicates that the roughness was lower than in as-cast nanocomposites (Figure 1av).

Figure 1 (ci) is the micrograph of 1.0 wt% MLG-EP nanocomposites processed with 1200P. The surface waviness (Figure 1cii) fluctuates in the range of ±10 µm while the surface roughness (Figure 1ciii) fluctuates in the range of ±10 µm. The roughness trend varies more rapidly than in as-cast samples and those processed with velvet cloth. However, the large notches have diminished. The Gaussian distribution (Figure 1civ) indicates that about uniform surface roughness was achieved with major size fraction of 2.2%. The roughness profile (Figure 1cv) indicates that there are no large surface notches.

Figure 1 (di) is the optical micrograph of 1.0 wt% MLG-EP processed with 320P. The scratches of different orientation and size were produced. The waviness (Figure 1dii) fluctuates in the range of ±20 µm while the roughness (Figure 1diii) fluctuates in the range of ±50 µm. The Gaussian distribution (Figure 1div) indicates that the major roughness fraction is 1.4%. The roughness profile (Figure 1dv) indicates that large notches emerge on the surface by processing with 320P.

Figure 1 (ei) is optical micrograph of 1.0 wt% MLG-EP processed with 60P. Coarse topographical features were achieved with high surface roughness. The waviness (Figure 1eii) fluctuates between ±30 µm while the surface roughness (Figure 1eiii) fluctuates in the range of ±100 µm. The deep sharp notches can be seen which significantly affect the mechanical performance of nanocomposites. The Gaussian distribution (Figure 1eiv) indicates that major fraction of surface roughness is 1.2%. The surface profile (Figure 1ev) shows the coarse topographical features with rapidly varying roughness. Similar results were observed for 1.0 wt% nanoclay- EP (Figure 2) and 0.5 wt% MLG-0.5 wt% nanoclay-EP samples (Figure 3).

The variation in mechanical performance with topography is shown in Figure 4. The densification of samples (Figure 4a) was around 99.5% and weight loss by treating abrasive papers (Figure 4b) was highest in case of 60P abrasive paper (16%). The microhardness (Figure 4c) increased in case of nanocomposites processed with velvet cloth and 1200P paper and decreased when samples were processed with 320P and 60P abrasive papers. The maximum microhardness was recorded in case of 0.5 wt% MLG- 0.5 wt% caly-EP samples. The Young's modulus (Figure 4d) increased in all cases when nanocomposites were processed with 1200P and velvet cloth. However, the stiffness decreased when the nanocomposites were processed with 320P and 60P abrasive papers. The values indicate that stiffness can be enhanced by processing the nanocomposites with velvet cloth and 1200P and degraded by processing the nanocomposites with 320P and 60P. The maximum increase in Young's modulus was observed in case of 0.5 wt% MLG-0.5 wt% nanoclay-EP nanocomposites and in case of nanocomposites processed with 1200P abrasive paper.

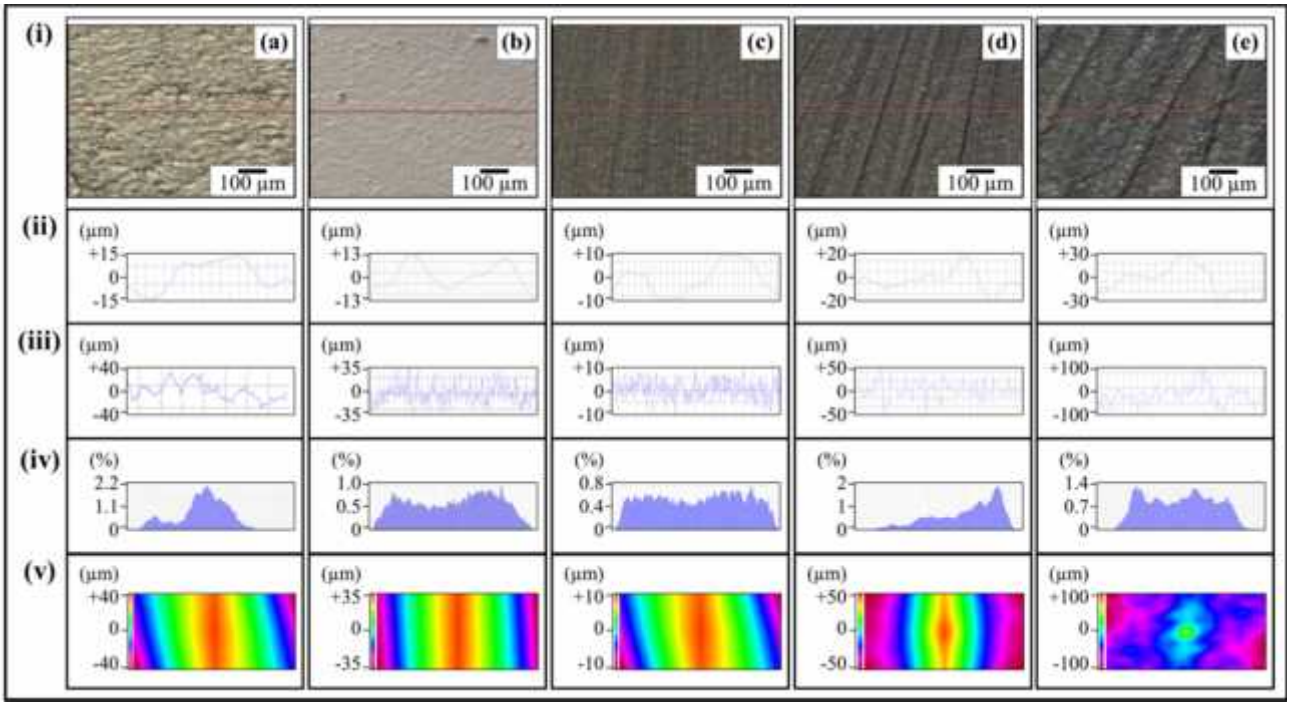

Figure 2. Topography profiles of 1.0 wt% nanoclay-EP samples: (a) As-cast; (b) Velvet cloth; (c) 1200P; (d) 320P; and (E) 60P abrasive papers. In all cases, (i) optical image, (ii) surface waviness, (iii) surface roughness (selected line), (iv) topographical dimensions vs. percentage, and (v) surface profile of selected region of nanocomposites.

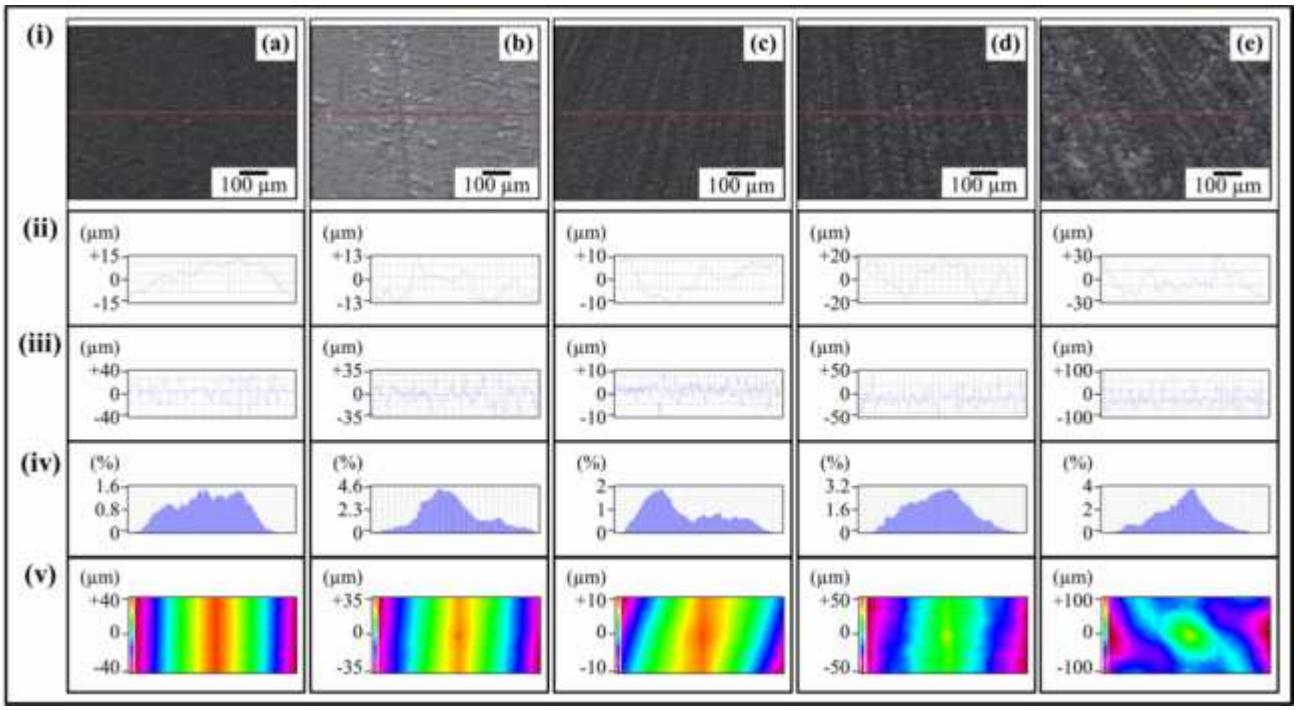

Figure 3. Topography profiles of 0.5 wt% MLG-0.5 wt% nanoclay-EP samples: (a) As-cast; (b) Velvet cloth; (c) 1200P; (d) 320P; and (E) 60P abrasive papers. In all cases, (i) optical image, (ii) surface waviness, (iii) surface roughness (selected line), (iv) topographical dimensions vs. percentage, and (v) surface profile of selected region of nanocomposites.

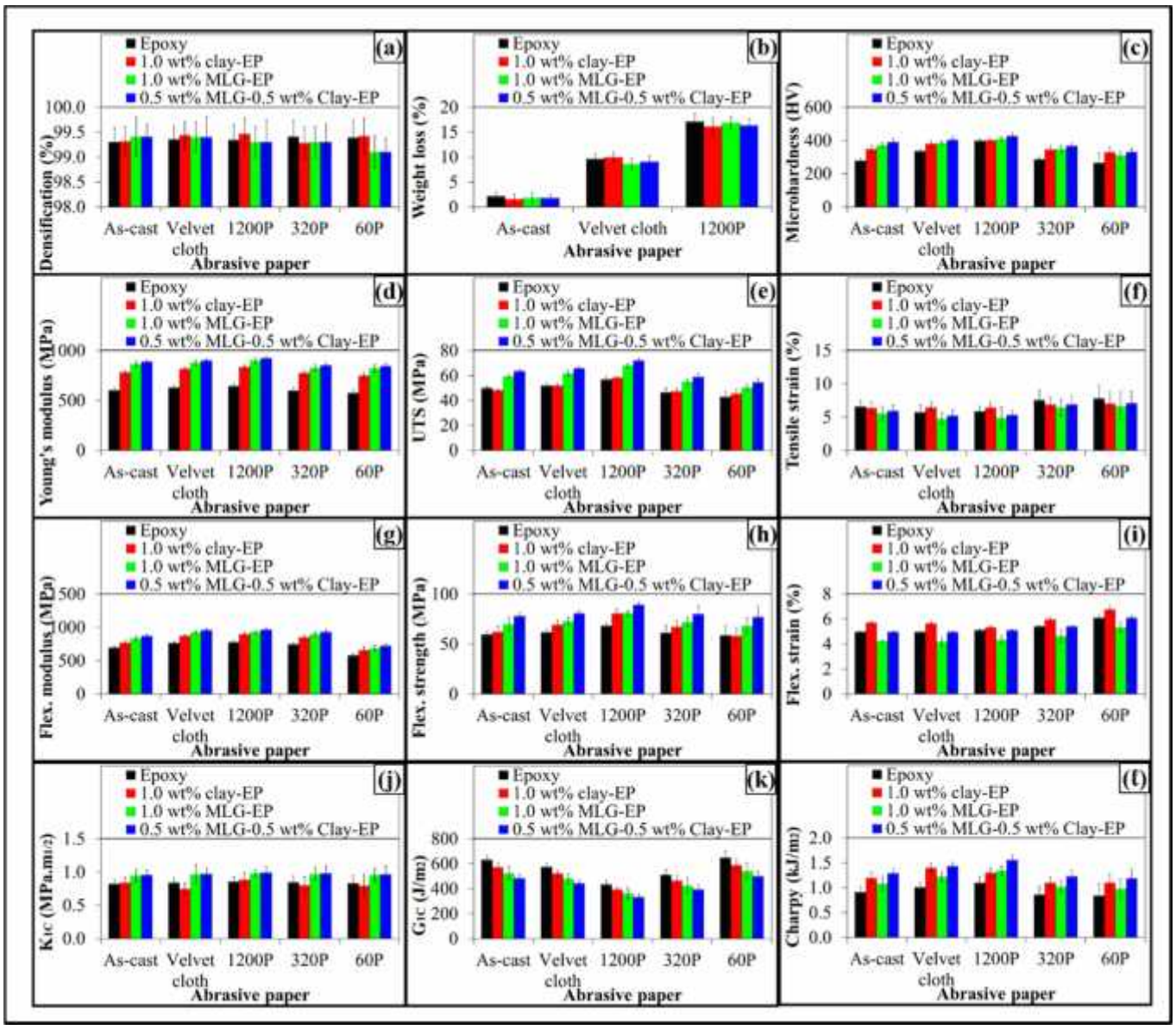

Figure 4. (a) Densification; (b) weight loss; (c) microhardness (d-ℓ) Mechanical performance of 1.0 wt% MLG/nanoclay-EP nanocomposites: (d) Young's modulus; (e) UTS; (f) tensile strain; (g) flexural modulus; (h) flexural strength; (i) flexural strain; (j) K_{1C}; (k) G_{1C}; and (ℓ) Charpy impact toughness.

The UTS (Figure 4e) also increased in all cases when nanocomposites were processed with 1200P abrasive paper and velvet cloth. However, the stiffness decreased when the nanocomposites were processed with 60P and 320P abrasive papers. The values show that UTS can be improved by treating the nanocomposites with 1200P abrasive paper and velvet cloth and decreased by treating the nanocomposites with 60P and 320P abrasive papers. The maximum increase in UTS was observed in case of 0.5 wt% MLG-0.5 wt% nanoclay-EP samples processed with 1200P.

The variation in tensile strain with topography is shown in Figure 4 (f). The tensile strain increased with high surface roughness values. It can be because of the reduction in strength and stiffness values. The treatment with velvet cloth did not show any visible change in tensile strain. However, the tensile strain slightly increased when the nanocomposites were processed with 1200P abrasive paper. Similar results were shown by nanocomposites when tested for flexural properties (Figure 4g-i). The values indicate that, from the three compositions made with five surface conditions for each composition, the best combination

of mechanical performance can be achieved in case of 0.5 wt% MLG-0.5 wt% nanoclay-EP nanocomposites processed with 1200P.

The variation in fracture toughness (K_{1C}) with topography is shown in Figure 4 (j). The K_{1C} remained impervious to any variation in topography. However, the standard deviation is not the same. It can be explained on the basis of tip of notch. A razor blade was used to sharpen the tip of notch that may not create tips of equal curvature and length. The other factor can be distribution, size, and volume fraction of porosity influencing the mechanical performance of nanocomposites. The variation in G_{1C} with topography is shown in Figure 4 (k). The G_{1C} increased with increasing surface roughness values. However, as K_{1C} remained impervious to topography, therefore, the variation in G_{1C} should not directly be a result of variation in topography. K_{1C}^2 was divided by stiffness to calculate G_{1C}. As stiffness decreased with increasing surface roughness values, therefore, a high value of G_{1C} resulted by increasing surface roughness. The variation in Charpy impact toughness with topography is shown in Figure 4 (ℓ). We believe that it is the stain rate which is different in K_{1C} and Charpy tests. The results indicate that surface roughness will be more influential in case of high strain rate (Charpy test) than at low strain rate (K_{1C} test).

The variation in dynamic mechanical performance with topography is shown in Figure 5. The maximum storage modulus values were shown by 0.5 wt% MLG-0.5 wt% clay-EP samples while the least were shown by 1.0 wt% clay-EP samples. The dynamic values corroborate the trends recorded in case of mechanical tests. It was further recorded that dynamic mechanical performance is not sensitive to any variation in topography.

The surface roughness of as-cast nanocomposites was ±43 µm (Figure 6a-d). The surface roughness of nanocomposites processed with velvet cloth and 1200P became ±33 µm and ±13 µm, respectively. Therefore, the increase in UTS and modulus can be related to the decrease in surface roughness values. Hence, stiffness and strength of nanocomposites can be improved by treating them with 1200P abrasive paper and velvet cloth. Furthermore, the surface roughness values of nanocomposites, processed with 320P and 60P abrasive papers, became ±52 µm and ±103 µm, respectively. Therefore, the decrease in strength and stiffness of nanocomposites by treating them with 60P and 320P abrasive paper can be related to the increase in surface roughness. From the surface roughness values, and details of mechanical performance, it can be stated that the roughness up to about ±20 µm is benign for mechanical performance of nanocomposites. Similarly, mechanical performance starts degrading when surface roughness exceeds ±20 µm.

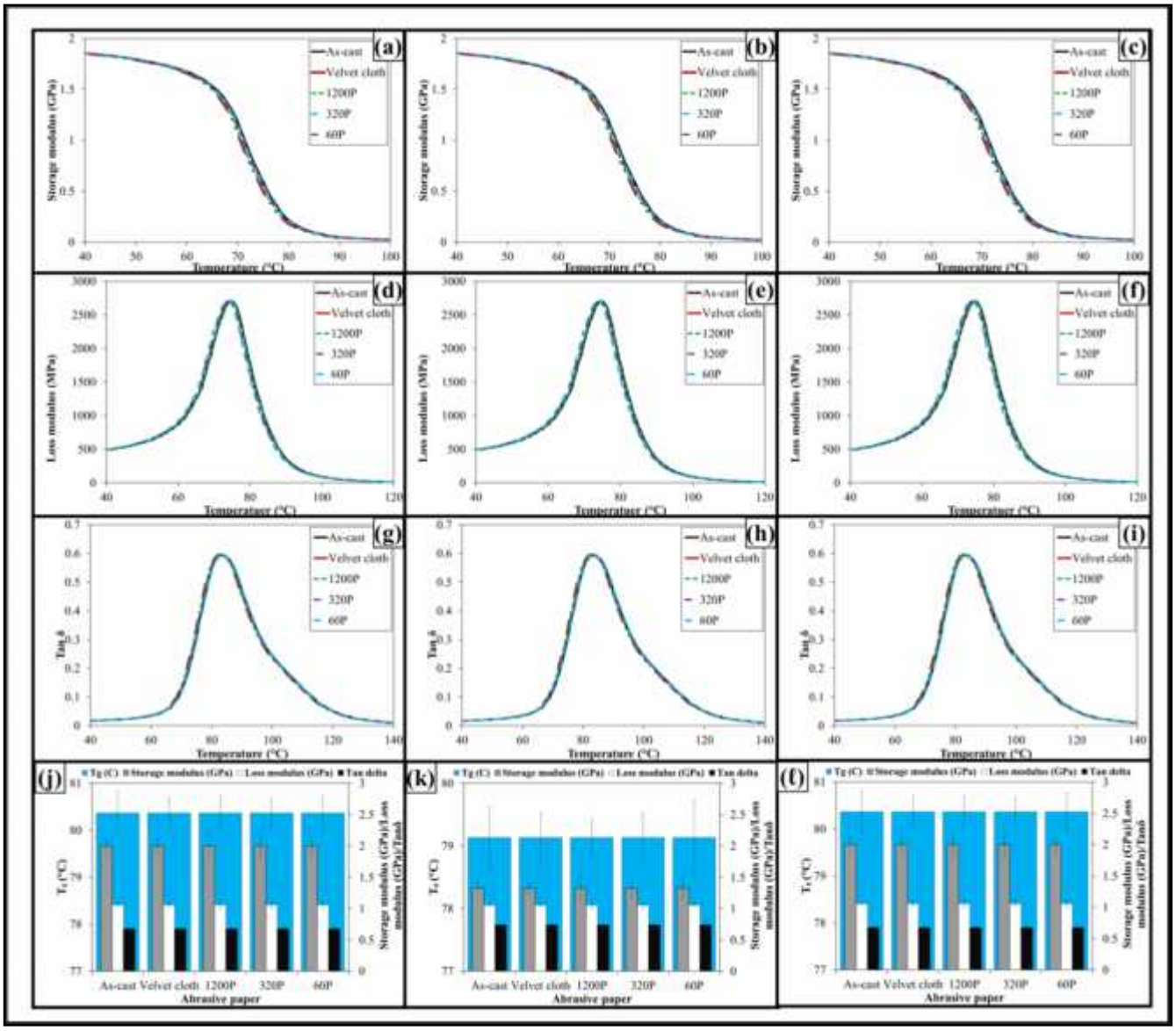

Figure 5. Dynamic mechanical performance of 1.0 wt% MLG-EP nanocomposites (left column), 1.0 wt% nanoclay-EP (middle column), and 0.5 wt% MLG-0.5 wt% nanoclay-EP (right column): (a,b,c) storage modulus, (d,e,f) loss modulus, (g,h,i) Tanδ (loss factor), and (j,k,ℓ) T_g, Tanδ, loss modulus, and storage modulus values corresponding to T_g.

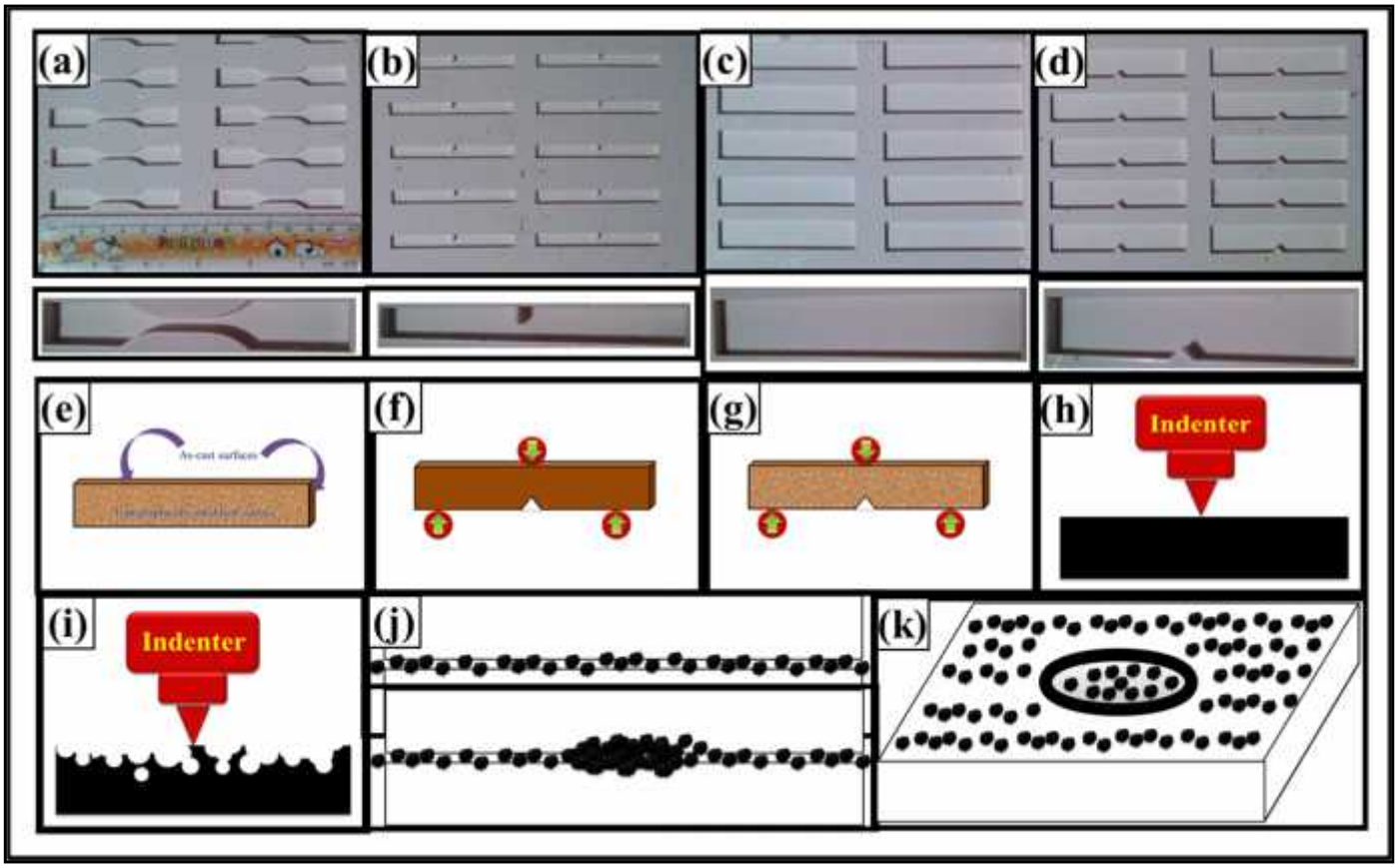

Figure 6. Mold photographs: (a) Tensile, (b) K_{1C} fracture toughness; (c) three-point bending; and (d) Charpy impact toughness. (e) Nanocomposites treated with abrasive papers, (f) as cast nanocomposite sample under bend load, (g) nanocomposite sample processed with abrasive paper. (h) High resistance offered to indenter by flat surface. (i) Rough and porous surface offers less resistance to indenter. (j) Debris formed during wear. (k) The coalesced debris result in crater.

The K_{1C} values of nanocomposites remained impervious to any variation in topography. It can be explained on the basis of loading axis and orientation of surface notches. The wider (bottom and top) surfaces of the nanocomposites were only processed with the abrasive papers. The thinner sides were not processed. Therefore, when bending loading was applied, the surfaces with coarse topography were oriented along the loading axis (Figure 6e-g). The size of the sample notch (3 mm) was much bigger than the surface notches generated by the abrasive papers (±100 µm). Therefore, the orientation of surface notches with respect to loading axis and the relative size of surface notches with respect to sample notch could possibly be the reasons that K_{1C} showed no variation with topography.

The increase in hardness can also be related to the variation in surface roughness. When surfaces are coarse, the indenter may sit at the edge of the ridge as shown in Figure 6 (h, i). In that case, less resistance will be observed by the material and hence low hardness will be recorded. This is a possible reason that low hardness was recorded in samples processed with 60P and 320P abrasive papers. On the other hand, when surfaces are smooth, strong resistance will be offered by the material against the penetration of indenter. In that case, high hardness will be observed. This could be the possible reason for high hardness observed in nanocomposites processed with 1200P abrasive paper and velvet cloth.

The UTS of as-cast 1.0 wt% MLG-EP samples is 59 MPa and of 1.0 wt% nanoclay-EP samples is 47 MPa. The microhardness and flexural properties showed similar trends. Therefore, MLG is more influential than nanoclay in enhancing the mechanical performance of the nanocomposites. The UTS of as-cast 1.0 wt% MLG-1.0 wt% nanoclay-EP samples is 63 MPa and is near to 1 wt% MLG-EP samples. Therefore, synergistic effects are not prominent enough at 1.0 wt% to yield a marked enhancement in mechanical performance of the nanocomposites.

The treatment of 1.0 wt% MLG/nanoclay-EP samples with abrasive papers produced topographical features with disparate orientation of surface notches, their shape and size. It can arise from the variation in surface roughness and size distribution of particles of the papers employed. Another momentous related phenomenon can be the formation of crater as shown in Figure 6 (j,k) [38]. When two surfaces are rubbed against each other, the extent of erosion depends on the roughness of the mating surfaces. Even the best polished surfaces show surface roughness at microscopic level [39]. When surfaces are smooth, the coefficient of friction is low. Hence, less erosion takes place. On the contrary, when the surfaces are coarse, the coefficient of friction is high. Hence, large erosion takes place. In addition to large erosion, there is possibility that the debris formed may not find a way to escape. In that case, they get trapped in between the mating surfaces. These debris may coalesce due to mechanical interlocking and cold welding. If surface energy is taken into account, then reduction in free energy could be a reason for coalescence. The coalesced debris are pressed against the mating surface and result in the formation of deep crater. This crater may significantly degrade the mechanical performance of mating surfaces by causing stress concentration. Hence, roughness above certain threshold may significantly deteriorate mechanical performance of nanocomposites. In case of polymer nanocomposites, the degree of crosslinking may be affected by the rise in temperature during friction. An increased degree of crosslinking can improve certain mechanical performance such as hardness and stiffness [11]. However, the fracture toughness showed an inverse relationship with the degree of crosslinking [40].

As air bubbles have lower density than that of epoxy, therefore, they tend to move out of the epoxy during curing. The velocity of air bubbles is directly proportional to the size of the air bubbles. Some of the air bubbles may escape the nanocomposites because of their higher velocity and proximity to the surface. However, those air bubbles that would not be able to escape will segregate near the surface such that the bigger bubbles will be closer to the surface than the smaller bubbles. The size of bigger bubbles may be large enough to cause a significant amount of stress concentration that can further cause deterioration in the mechanical performance. Therefore, removing the material from the surface will remove the areas with majority of defects. The presence of air bubbles next to the surface can be witnessed in the literature [41]. Warrier et al. produced carbon nanotubes filled epoxy nanocomposites using vacuum bagging. They reported that air bubbles were concentrated on the edges of produced surfaces [41]. They further reported that CNT reinforced samples had more air bubbles than those without CNT [41]. Some of the authors have also shown that air bubbles are retained in nanocomposites produced using solution casting technique [25,42]. Once the surface material is removed, then not only the surface notches can be eradicated, but also the regions with air bubbles. A similar technique is used in forged and cast metals and alloys. For example, forged steel contains scale at its surface arising from the reaction of iron with oxygen at high temperature which produces iron oxide. The forged steel parts are machined to remove undesired materials as well as to get surface of required finish. Therefore, removing surface material may help improve mechanical performance of polymer nanocomposites.

4. Conclusions:

The topography can significantly influence the mechanical performance of epoxy nanocomposites. The tensile properties start degrading when surface notches exceed ±20 µm. However, flexural properties are less sensitive to topography than tensile properties and start degrading after ±50 µm. The UTS of 1.0 wt% MLG-EP samples (as-cast) is 59 MPa and of 1.0 wt% nanoclay-EP samples is 47 MPa. The microhardness and flexural properties showed similar trends. Therefore, MLG is more influential than nanoclay in enhancing the mechanical performance of epoxy nanocomposites. The UTS of 1.0 wt% MLG-1.0 wt% nanoclay-EP samples (as-cast) is 63 MPa and is near to 1 wt% MLG-EP samples. Therefore, synergistic effects are too weak at 1.0 wt% to yield a marked enhancement in mechanical performance of the nanocomposites. The topography did not vary the dynamic mechanical performance.

5. Acknowledgements:

The authors would like to thank the Department of Mechanical and Construction Engineering, Northumbria University, UK for the provision of research facilities, without which the analysis of relevant data was not possible.

6. References:

[1] Schuler M, Kunzler TP, De Wild M, Sprecher CM, Trentin D, Brunette DM, et al. Fabrication of TiO2-coated epoxy replicas with identical dual-type surface topographies used in cell culture assays. J Biomed Mater Res - Part A 2009;88:12–22. doi:10.1002/jbm.a.31720.

[2] Lam CK, Lau KT. Tribological behavior of nanoclay/epoxy composites. Mater Lett 2007;61:3863–6. doi:10.1016/j.matlet.2006.12.078.

[3] Yu S, Hu H, Ma J, Yin J. Tribological properties of epoxy/rubber nanocomposites. Tribol Int 2008;41:1205–11. doi:10.1016/j.triboint.2008.03.001.

[4] Atif R, Inam F. Influence of Macro-Topography on Damage Tolerance and Fracture Toughness of 0.1 wt%Multi-Layer Graphene/Clay-Epoxy Nanocomposites. Polymers (Basel) 2016;239:335–60. doi:10.3390/polym8070239.

[5] Atif R, Inam F. Influence of Macro-Topography on Damage Tolerance and Fracture Toughness of Monolithic Epoxy for Tribological Applications. World J Eng Technol 2016:335–60.

[6] Siegel R, Hu E, Roco M, Editors. Nanostructure science and technology. A worldwide study. Prepared under the guidance of the IWGN, NSTC. WTEC. 1999.

[7] Pan G, Guo Q, Ding J, Zhang W, Wang X. Tribological behaviors of graphite/epoxy two-phase composite coatings. Tribol Int 2010;43:1318–25. doi:10.1016/j.triboint.2009.12.068.

[8] Brostow W, Dutta M, Rusek P. Modified epoxy coatings on mild steel: Tribology and surface energy. Eur Polym J 2010;46:2181–9. doi:10.1016/j.eurpolymj.2010.08.006.

[9] Zhang WH, Hsieh JH. Tribological behavior of TiN and CrN coatings sliding against an epoxy molding compound. Surf Coatings Technol 2000;130:240–7. doi:10.1016/S0257-8972(00)00709-X.

[10] Chang L, Zhang Z, Ye L, Friedrich K. Tribological properties of epoxy nanocomposites. III. Characteristics of transfer films. Wear 2007;262:699–706. doi:10.1016/j.wear.2006.08.002.

[11] Lackner JM, Waldhauser W, Ganser C, Teichert C, Kot M, Major L. Mechanisms of topography formation of magnetron-sputtered chromium-based coatings on epoxy polymer composites. Surf Coatings Technol 2014;241:80–5. doi:10.1016/j.surfcoat.2013.07.040.

[12] Yao XF, Zhou D, Yeh HY. Macro/microscopic fracture characterizations of SiO2/epoxy nanocomposites. Aerosp Sci Technol 2008;12:223–30. doi:10.1016/j.ast.2007.03.005.

[13] Wetzel B, Rosso P, Haupert F, Friedrich K. Epoxy nanocomposites - fracture and toughening mechanisms. Eng Fract Mech 2006;73:2375–98. doi:10.1016/j.engfracmech.2006.05.018.

[14] Naous W, Yu XY, Zhang QX, Naito K, Kagawa Y. Morphology, tensile properties, and fracture toughness of epoxy/Al2O3 nanocomposites. J Polym Sci Part B-Polymer Phys 2006;44:1466–73. doi:10.1002/Polb.20800.

[15] Kim BC, Park SW, Lee DG. Fracture toughness of the nano-particle reinforced epoxy composite. Compos Struct 2008;86:69–77. doi:10.1177/0892705714556835.

[16] Wang K, Chen L, Wu J, Toh ML, He C, Yee AF. Epoxy nanocomposites with highly exfoliated clay: Mechanical properties and fracture mechanisms. Macromolecules 2005;38:788–800. doi:10.1021/ma048465n.

[17] Liu W, Hoa S V., Pugh M. Fracture toughness and water uptake of high-performance epoxy/nanoclay nanocomposites. Compos Sci Technol 2005;65:2364–73. doi:10.1016/j.compscitech.2005.06.007.

[18] Gojny FH, Wichmann MHG, Köpke U, Fiedler B, Schulte K. Carbon nanotube-reinforced epoxy-composites: Enhanced stiffness and fracture toughness at low nanotube content. Compos Sci Technol 2004;64:2363–71. doi:10.1016/j.compscitech.2004.04.002.

[19] Yu N, Zhang ZH, He SY. Fracture toughness and fatigue life of MWCNT/epoxy composites. Mater Sci Eng A 2008;494:380–4. doi:10.1016/j.msea.2008.04.051.

[20] Srikanth I, Kumar S, Kumar A, Ghosal P, Subrahmanyam C. Effect of amino functionalized MWCNT on the crosslink density, fracture toughness of epoxy and mechanical properties of carbon-epoxy composites. Compos Part A Appl Sci Manuf 2012;43:2083–6. doi:10.1016/j.compositesa.2012.07.005.

[21] Mathews MJ, Swanson SR. Characterization of the interlaminar fracture toughness of a laminated carbon/epoxy composite. Compos Sci Technol 2007;67:1489–98. doi:10.1016/j.compscitech.2006.07.035.

[22] Arai M, Noro Y, Sugimoto K ichi, Endo M. Mode I and mode II interlaminar fracture toughness of CFRP laminates toughened by carbon nanofiber interlayer. Compos Sci Technol 2008;68:516–25. doi:10.1016/j.compscitech.2007.06.007.

[23] Wong DWY, Lin L, McGrail PT, Peijs T, Hogg PJ. Improved fracture toughness of carbon fibre/epoxy composite laminates using dissolvable thermoplastic fibres. Compos Part A Appl Sci Manuf 2010;41:759–67. doi:10.1016/j.compositesa.2010.02.008.

[24] Atif R, Wei J, Shyha I, Inam F. Use of morphological features of carbonaceous materials for improved mechanical properties of epoxy nanocomposites. RSC Adv 2016;6:1351–9. doi:10.1039/C5RA24039E.

[25] Atif R, Shyha I, Inam F. The degradation of mechanical properties due to stress concentration caused by retained acetone in epoxy nanocomposites. RSC Adv 2016;6:34188–97. doi:10.1039/C6RA00739B.
[26] Atif R, Shyha I, Inam F. Modeling and experimentation of multi-layered nanostructured graphene-epoxy nanocomposites for enhanced thermal and mechanical properties. J Compos Mater 2016:1–12. doi:10.1177/0021998316640060.
[27] Atif R, Inam F. Modeling and Simulation of Graphene Based Polymer Nanocomposites : Advances in the Last Decade. Graphene 2016:96–142. doi:http://dx.doi.org/10.4236/graphene.2016.52011.
[28] Sumfleth J, de Almeida Prado LAS, Sriyai M, Schulte K. Titania-doped multi-walled carbon nanotubes epoxy composites: Enhanced dispersion and synergistic effects in multiphase nanocomposites. Polymer (Guildf) 2008;49:5105–12. doi:10.1016/j.polymer.2008.09.016.
[29] Ma H, Tong L, Xu Z, Fang Z. Synergistic effect of carbon nanotube and clay for improving the flame retardancy of ABS resin. Nanotechnology 2007;18:375602. doi:10.1088/0957-4484/18/37/375602.
[30] Cotell CM, Sprague JA, Smidth FAJ, editors. ASM Handbook, Vol. 5. Surface Engineering. 1994.
[31] Karger-Kocsis J, Mahmood H, Pegoretti A. Recent advances in fiber/matrix interphase engineering for polymer composites. Prog Mater Sci 2015;73:1–43. doi:10.1016/j.pmatsci.2015.02.003.
[32] Moon SI, Jang J. Mechanical interlocking and wetting at the interface between argon plasma treated UHMPE fiber and vinylester resin. J Mater Sci 1999;34:4219–24. doi:10.1023/A:1004642500738.
[33] Nardin M, Ward IM. Influence of surface treatment on adhesion of polyethylene fibres. Mater Sci Technol 1987;3:814–26. doi:10.1179/mst.1987.3.10.814.
[34] Ladizesky NH, Ward IM. The adhesion behaviour of high modulus polyethylene fibres following plasma and chemical treatment. J Mater Sci 1989;24:3763–73. doi:10.1007/BF02385768.
[35] Woods DW, Ward IM. Study of the oxygen treatment of high-modulus polyethylene fibres. Surf Interface Anal 1993;20:385–392. doi:10.1002/sia.740200510.
[36] Tissington B, Pollard G, Ward IM. A study of the influence of fibre/resin adhesion on the mechanical behaviour of ultra-high-modulus polyethylene fibre composites. J Mater Sci 1991;26:82–92. doi:10.1007/BF00576036.
[37] Engelke R, Engelmann G, Gruetzner G, Heinrich M, Kubenz M, Mischke H. Complete 3D UV microfabrication technology on strongly sloping topography substrates using epoxy photoresist SU-8. Microelectron Eng 2004;73–74:456–62. doi:10.1016/j.mee.2004.03.017.
[38] Pitler RK, Langer EL, editors. ASM Handbook, Vol. 16. Machining. 1995.
[39] Blau PJ, editor. ASM Handbook, Vol. 18. Friction, Lubrication, and Wear Technology. 2001.
[40] Wang X, Jin J, Song M. An investigation of the mechanism of graphene toughening epoxy. Carbon N Y 2013;65:324–33. doi:10.1016/j.carbon.2013.08.032.
[41] Warrier A, Godara A, Rochez O, Mezzo L, Luizi F, Gorbatikh L, et al. The effect of adding carbon nanotubes to glass/epoxy composites in the fibre sizing and/or the matrix. Compos Part A Appl Sci Manuf 2010;41:532–8. doi:10.1016/j.compositesa.2010.01.001.
[42] Rasheed A, Khalid FA. Fabrication and properties of CNTs reinforced polymeric matrix nanocomposites for sports applications. IOP Conf Ser Mater Sci Eng 2014;60:12009. doi:10.1088/1757-899X/60/1/012009.